

raf RBD and Ubiquitin Proteins Share Similar Folds, Folding Rates and Mechanisms Despite Having Unrelated Amino Acid Sequences[†]

Alexis Vallée-Bélisle, Jean-François Turcotte, and Stephen W. Michnick*

Département de biochimie, Université de Montréal, CP 6128, Station Centre-Ville, Montréal, Québec H3C 3J7, Canada

Received October 30, 2003; Revised Manuscript Received April 22, 2004

ABSTRACT: Recent experimental and theoretical studies in protein folding suggest that the rates and underlying mechanisms by which proteins attain the native state are largely determined by the topological complexity of a specific fold rather than by the fine details of the amino acid sequences. However, such arguments are based upon the examination of a limited number of protein folds. To test this view, we sought to investigate whether proteins belonging to the ubiquitin superfamily display similar folding behavior. To do so, we compared the folding–unfolding transitions of mammalian ubiquitin (mUbi) with those of its close yeast homologue (yUbi), and to those of the structurally related Ras binding domain (RBD) of the serine/threonine kinase *raf* that displays no apparent sequence homology with the ubiquitin family members. As demonstrated for mUbi [Krantz, B. A., and Sosnick, T. R. (2000) *Biochemistry* 39, 11696–11701], we show that a two-state transition model with no burst phase intermediate can describe folding of both yUbi and *raf* RBD. We further demonstrate that (1) all three proteins refold at rates that are within 1 order of magnitude (1800, 1100, and 370 s⁻¹ for mUbi, *raf* RBD, and yUbi, respectively), (2) both mUbi and *raf* RBD display similar refolding heterogeneity, and (3) the folding free energy barriers of both mUbi and *raf* RBD display a similar temperature dependence and sensitivity to a stabilizing agent or to mutations of a structurally equivalent central core residue. These findings are consistent with the view that rates and mechanisms for protein folding depend mostly on the complexity of the native structure topology rather than on the fine details of the amino acid sequence.

During the past decade, simplifying concepts of protein folding behavior have emerged from the study of many single-domain, two-state folding proteins (1–9). A key finding has been that the complexity of the native-state search (measured by the folding rate of a protein) is, surprisingly, correlated to a “contact order”, a parameter which quantifies the average sequence separation that exists between residues making contact in the native structure of a protein (10). The existence of such a correlation between a parameter that describes the complexity of structural topologies and folding rate is supported by both experimental and theoretical evidence. Experimentally, folding rates of homologous proteins (11) and highly mutated variants (12, 13) were found to be relatively similar, and transition-state structures, characterized by ϕ value analysis, of structurally homologous protein pairs have been found to be conserved (14–16). On a theoretical basis, several studies using low-resolution models with G \ddot{o} -like approximations could be used to predict folding rates and the folding transition-state structure with good success (17–19). These results highlight the importance of native-state topology versus fine details of the polypeptide chain sequence as a determinant of protein folding rates and mechanisms (4).

However, these arguments are built upon studies of a limited number of protein folds. Furthermore, folding studies

comparing structurally related members often involved proteins, which have a discernible sequence homology (i.e., similarities in their fine sequence details) (11–13, 15, 16, 21, 22). In the study presented here, we thus sought to examine whether folding rates and mechanisms of structurally related members belonging to the ubiquitin superfamily are similar in the absence of apparent amino acid sequence conservation. We chose the ubiquitin-like topology as a model for two reasons. First, the ubiquitin superfamily represents a remarkable example of structural versatility: its members display large sequence variation, various binding surface locations, and many unrelated functions (23). In a recent version of the SCOP database (May 2003), where structures are grouped by fold, superfamilies, and families, up to six sequence-distant families exhibit the characteristic ubiquitin-like $\beta\beta\alpha\beta\beta\alpha\beta$ secondary structure arrangement (24). Second, the folding of mammalian ubiquitin (mUbi)¹ has been studied extensively over the past decade, but the interpretation of its folding mechanism has remained the subject of controversy. In the mid-1990s, Roder and co-workers reported the existence of a putative “burst phase” intermediate in the refolding of mUbi^{F45W} at a low denaturant concentration (a transition thought to take place during the mixing period of the stopped-flow apparatus), which also appeared to be correlated with a rate constant rollover at 25 °C (25, 26). The authors proposed that their results could

[†] This work was supported by The Natural Sciences and Engineering Research Council of Canada (Grant 194582-00).

* To whom correspondence should be addressed. Phone: (514) 343-5849. Fax: (514) 343-2015. E-mail: stephen.michnick@umontreal.ca.

¹ Abbreviations: mUbi, mammalian ubiquitin; yUbi, yeast ubiquitin; *raf* RBD, Ras binding domain of the serine/threonine kinase *raf*; Gdn-HCl, guanidine hydrochloride; CD, circular dichroism.

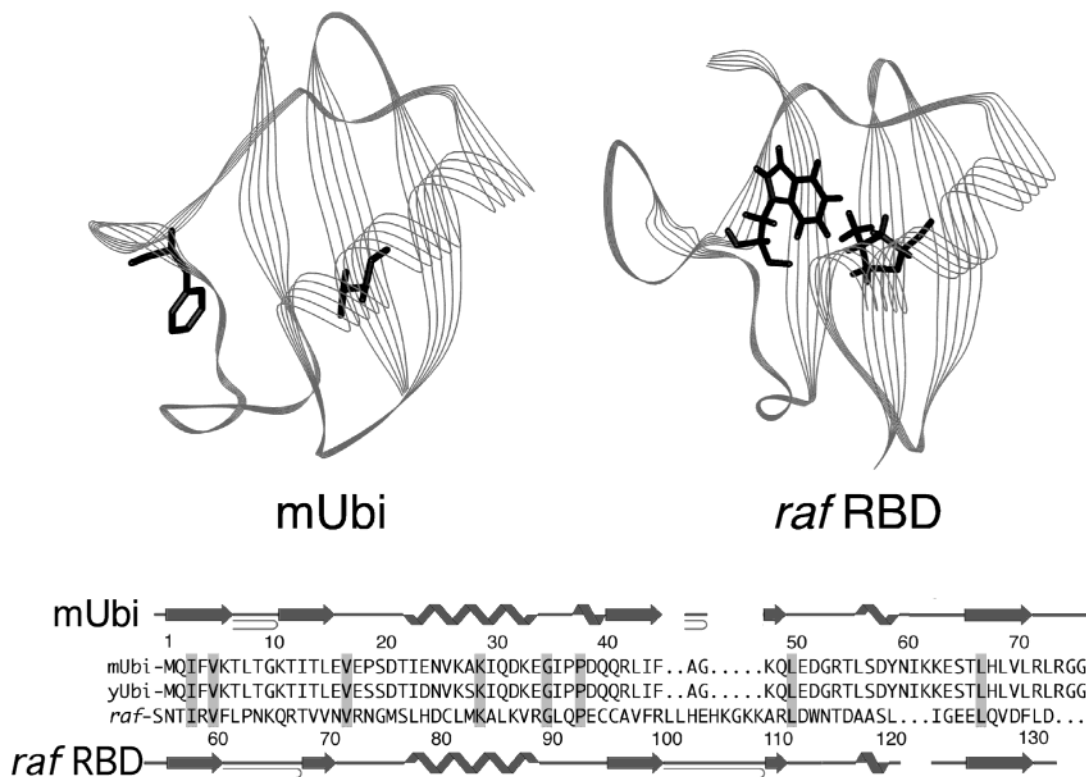


FIGURE 1: Tertiary and secondary ribbon structures of mUbi and *raf* RBD and their primary structure alignment. Amino acids with displayed side chains include Phe 45 and Val 26 for mUbi and Trp 114 and Leu 82 for *raf* RBD. Phe 45, mutated in this study to Trp, and WT Trp 114 of *raf* RBD were used as fluorescent probes to monitor the folding–unfolding transitions, while Val 26 and Leu 82 correspond to the structurally equivalent central hydrophobic residues that were mutated in previous studies and this study. The alignment of the primary structures was derived from both tertiary (31) and secondary structure alignments. The tertiary and secondary structure representations were based on solution structures of the proteins using WebLab ViewerLite version 3.2 and PDBsum (48), respectively (PDB entries 1UBI and 1RFA).

be fit to a three-state model and interpreted as support for the existence of an early hydrophobic intermediate that is rapidly populated at the initiation of folding (27). On the other hand, Krantz and Sosnick have recently demonstrated that a two-state model could adequately describe the folding mechanism for mUbi under conditions in which the fastest phase is not lost in the dead time of the stopped-flow apparatus (28, 29). Studies of additional ubiquitin superfamily members could thus aid in resolving this controversy.

For these reasons, we decided to compare the folding–unfolding pathway of mUbi to that of its close *Saccharomyces cerevisiae* yeast homologue, yUbi (sequence 96% identical), and, by contrast, to that of a structurally related protein displaying no apparent sequence homology with the ubiquitin proteins (Figure 1). Among the different superfamily members, *raf* RBD was identified as a good model for these studies because (1) its topology is virtually identical to that of ubiquitin, despite an apparent lack of sequence identity (<11%) (30, 31), (2) it contains a single, partially buried tryptophan residue that could provide a fluorescent probe for monitoring the folding–unfolding transition (see Trp 114 in Figure 1), (3) it does not contain covalent disulfide bonds, and (4) it has two proline residues, Pro 64 and Pro 93, which are fixed in a *trans* conformation in the native structure of the protein, thus ensuring that only a small ratio of unfolded protein will be trapped in the slow rate-limiting prolyl isomerization at the initiation of refolding (32).

In this work, we demonstrate that the folding–unfolding transition of the ubiquitin family and superfamily members mUbi, yUbi, and *raf* RBD can be described well by an apparent two-state model, refold with similar rate constants, and show similar refolding heterogeneity. To further compare the folding mechanism of sequence-unrelated mUbi and *raf* RBD, we then present evidence to demonstrate that both proteins display equivalent folding free energy barrier variations when subjected to the same set of perturbations. Our results suggest that these proteins fold via similar folding pathways and thus reinforce the idea that the folding energy landscapes of proteins are relatively insensitive to the fine details of the amino acid sequences.

MATERIALS AND METHODS

Protein Constructions and Expression. The yUbi coding sequence was amplified by a standard PCR procedure from the *Sal*I engineered *Saccharomyces cerevisiae* UB14-derived Ubi gene (33) and cloned without further amino acid addition into a modified version of *Escherichia coli* expression plasmid pQE-32 (Qiagen). The mUbi coding sequence was obtained by (1) amplifying the yUbi cDNA using a 5′ oligonucleotide which contains mUbi amino acid mutations (S19P, D22E, and S28A) and (2) cloning the PCR product into the yUbi expression vector using the *Age*I site, which encodes amino acid positions 9 and 10 of the yUbi coding sequence. The Phe 45 → Trp mutation was introduced into both ubiquitin coding sequences by replacing the wild-type

(WT) nucleotides using a megaprimer PCR strategy (34). The *raf* RBD coding sequence was amplified by a standard PCR procedure from the pWD333 plasmid (35), and cloned into a modified version of pQE-32 with two extra amino acids added at the N-terminal extremity of the coding sequence (MG). Mutants L82I, L82V, and L82A were amplified from the parental sequence using a megaprimer PCR strategy (34) to replace the appropriate nucleotides and cloned back into the WT *raf* RBD expression vector. Coding sequence mUbi^{F45W} and *raf* RBD were alternatively cloned into a modified version of pQE-32 containing a polyhistidine tag. His₆-mUbi^{F45W} and His₆-*raf* RBD thus contain the following amino acid insertions at their N-termini: MHH-HHHHG and MHHHHHSMG, respectively. The coding sequences and promoter of the different expression vectors were verified by sequencing. Expression vectors were transformed into *E. coli* BL21 strain containing the *lacI* repressor in *trans* on a separate pREP4 plasmid. Cell cultures in ampicillin- and kanamycin-containing media were grown to an OD₆₀₀ of 0.8, and induced with 1 mM IPTG. After growing for 6 h, the cells were harvested by centrifugation and flash-frozen in liquid nitrogen.

Protein Purification. All proteins were resuspended in a minimal amount of buffer A [50 mM Tris-HCl (pH 8.0)] and sonicated on ice in 5 mL samples (~4% of buffer A per culture volume). His-tagged proteins (used for double-jump experiments only) were purified at a high concentration (~500 μM) with Ni-NTA resin using the standard manufacturer's procedures (Qiagen). The eluted protein solution was then subjected to extensive dialysis to eliminate traces of imidazole. Purification of untagged proteins started with the addition of 50 mM MnCl₂ to precipitate DNA followed by a centrifugation to remove cell debris (these were recovered for mutant *raf* RBD L82A; see below). For the ubiquitin proteins, the supernatant was heated for 5 min at 80 °C and rapidly cooled, and the precipitated protein was removed by a second centrifugation. Purification was carried out with an 80% ammonium sulfate precipitation at 4 °C followed by size exclusion chromatography on a Sephadex G50 column (Pharmacia). The typical yield was 50 mg of pure protein/L as confirmed by Tricine SDS-PAGE. Purification of WT *raf* RBD and both mutants L82I and L82V was carried out by (1) applying the supernatant on a 15 mL cationic resin (S Sepharose from Pharmacia) equilibrated in buffer A (*raf* RBD pK_i ~ 8.9), (2) eluting *raf* RBD with 200–250 mM NaCl fractions using a NaCl gradient, (3) concentrating the protein by ammonium sulfate precipitate (80% at 4 °C) and resuspending it in a minimum amount of buffer B [50 mM Tris-HCl (pH 7.5) and 0.5 mM DTT], and (4) applying the concentrated *raf* RBD sample to a Sephadex G50 column (Pharmacia). Purification of mutant L82A was carried out by (1) washing cell debris with 50 mL of buffer A and recovering the pellet from a second centrifugation, (2) resuspending this pellet in buffer C [6 M urea, 50 mM Tris-HCl (pH 8.0), and 0.5 mM DTT] and recovering the supernatant from a third centrifugation, (3) applying the supernatant on a 10 mL cationic resin (S Sepharose from Pharmacia) equilibrated in buffer C, (4) eluting *raf* RBD with 200–250 mM NaCl fractions using a NaCl gradient in buffer C, (5) reducing the urea concentration using dialysis against a 20× volume of buffer D [0.4 M Na₂SO₄ (enzyme grade from Fisher), 50 mM Tris-HCl (pH 7.5), and 0.5 mM DTT]

and precipitating the L82A mutant with 80% ammonium sulfate at 4 °C, and (6) resuspending the protein pellet with buffer E [2.5 M Gdn-HCl (ultrapure grade from ICN), 50 mM Tris-HCl (pH 7.5), and 0.5 mM DTT] and applying it on a Sephadex G50 column (Pharmacia) equilibrated with buffer E. The fraction containing the protein was further subjected to dialysis using buffer B or buffer E for unfolding or folding experiments, respectively. The protein purity was confirmed with Tricine SDS-PAGE and the protein concentration later adjusted using Biomax-5 kDa Ultrafree centrifugal filter device (Millipore). The typical yield was 50 mg of pure protein/mL for WT *raf* RBD and mutants.

Data Collection. All experiments were performed in 25 mM sodium acetate buffer (pH 5.0) (ubiquitins) or in 50 mM Tris buffer (pH 7.5) with 0.5 mM DTT (*raf* RBD). The temperature was kept constant at 25 ± 0.1 °C unless otherwise specified. All measurements were taken using an Applied Photophysics SX18.MV stopped-flow fluorimeter with excitation wavelengths set to 285 nm (ubiquitins) or 281 nm (*raf* RBD) with a bandwidth of 2.5 nm. Fluorescence emission spectra were monitored by taking fluorescence measurements every 2 nm between 300 and 400 nm using a bandwidth of 5 nm, while equilibrium and kinetic denaturant dependence studies were performed by reading fluorescence intensity using a high-pass glass filter with 320 nm (ubiquitins) or 305 nm (*raf* RBD) cutoffs. All equilibrium stability curves were generated by using the equilibrium end point of 10 s for folding or unfolding kinetic traces. Three 10 s relaxation traces, each containing 1000 data points distributed in a logarithmic scale, were averaged for all kinetic experiments. Refolding experiments were carried out by mixing 1 volume of the denatured protein (in 6.0 or 4.5 M Gdn-HCl solutions for ubiquitin proteins or *raf* RBD, respectively) with 10 volumes of solutions with denaturant concentrations ranging from 0 to 7.0 M. Unfolding experiments were performed by mixing 1 volume of native protein (in 1.0 or 0.5 M Gdn-HCl solutions for the ubiquitins or *raf* RBD, respectively) with 10 volumes of solutions with denaturant concentrations ranging from 7.0 to 0 M. Kinetic experiments performed on the *raf* RBD L82A mutant required different conditions because of its low stability. The unfolded sample only required a 2.0 M Gdn-HCl solution, while in the unfolding experiment, a 1:1 mixing was used to prevent aggregation by lowering the concentration of the protein sample. The final Gdn-HCl concentration of each experiment was determined by refractive index measurements with an Abbe 60 refractometer (Bellingham & Stanley Ltd.) using an independent set of dilutions. Final protein concentrations employed in single-jump experiments were set to approximately 20 or 15 μM for the ubiquitins or *raf* RBD based on an extinction coefficient of 6990 or 5875 M⁻¹ at 280 nm, respectively (36). His-tagged proteins were used in double-jump experiments because they could be purified at the much higher concentrations required to achieve the 1:77 dilution of protein needed in these experiments. These began with rapidly unfolding 2 volumes of native His-tagged proteins (in 1.0 M and 0.5 M Gdn-HCl for mUbi and *raf* RBD, respectively) in 5 volumes of concentrated Gdn-HCl solutions (8.0 and 6.3 M Gdn-HCl for mUbi and *raf* RBD, respectively). After a 10 s delay, these samples were then subjected to rapid refolding using 1:10 mixing with low denaturant concentrations. Final protein concentrations em-

ployed in double-jump experiments were set to approximately 10 μM .

Equilibrium analysis using a two-state model of denaturation, in which only the native and denatured states are populated at equilibrium (see eq 1), was applied to the entire set of fluorescence data extrapolated to infinity ($F_{\infty}^{\text{Gdn-HCl}}$) using the fit made on the kinetic traces in the denaturant unfolding and refolding studies (see Kinetic Analysis).

$$F_{\infty}^{\text{Gdn-HCl}} = [F_{\text{N}}^{\text{Gdn-HCl}} + F_{\text{U}}^{\text{Gdn-HCl}} \exp(m\text{Gdn-HCl} - \Delta G^{\text{H}_2\text{O}})/RT] / [1 + \exp(m\text{Gdn-HCl} - \Delta G^{\text{H}_2\text{O}})/RT] \quad (1)$$

Equation 1 assumes that the fluorescence intensity of the native and unfolded states ($F_{\text{N}}^{\text{Gdn-HCl}}$ and $F_{\text{U}}^{\text{Gdn-HCl}}$) are linear functions of Gdn-HCl concentration (Gdn-HCl). The model also assumes that the difference in free energy between the denatured and native states (ΔG) varies linearly with the denaturant concentration, with a slope of m . $\Delta G^{\text{H}_2\text{O}}$ represents the difference in free energy between the two states in the absence of denaturant. The fraction of folded protein (F_{N}) was obtained from the raw stability curve data using the following transformation:

$$F_{\text{N}} = (F_{\infty}^{\text{Gdn-HCl}} - F_{\text{U}}^{\text{Gdn-HCl}}) / \{1 + \exp[(m\text{Gdn-HCl} - \Delta G^{\text{H}_2\text{O}})/RT]\} / F_{\text{N}}^{\text{Gdn-HCl}} \quad (2)$$

Kinetic Analysis. Following the dead time determination of the stopped-flow apparatus (37), all the kinetic traces were transformed by adding 0.7 ms (proper setting of the initial reaction time) and removing all experimental data acquired before 3.5 ms. Kinetic parameters of the different traces were obtained by using the nonlinear regression analysis program Kaleidagraph (version 3.6, Synergy Software). All unfolding kinetic traces could be described well by either a single exponential or a constant function (unfolding experiments carried out under native conditions). Folding kinetic traces could require up to four exponential terms at low denaturant concentrations to be properly fit. Relaxation rates observed for the unfolding and the major refolding transitions were fit to a two-state model (chevron curve) according to eq 3.

$$\ln k_{\text{obs}} = \ln[k_{\text{F}}^{\text{H}_2\text{O}} \exp(-m_{\text{F}}\text{Gdn-HCl}) + k_{\text{U}}^{\text{H}_2\text{O}} \exp(-m_{\text{U}}\text{Gdn-HCl})] \quad (3)$$

The observed relaxation rate, k_{obs} , is the sum of the refolding and unfolding rates (k_{F} and k_{U} , respectively) at any Gdn-HCl concentration. The logarithms of k_{F} and k_{U} are assumed to be linear functions of the denaturant concentration with slopes m_{F} and m_{U} , respectively. $k_{\text{F}}^{\text{H}_2\text{O}}$ and $k_{\text{U}}^{\text{H}_2\text{O}}$ are the rates of folding and unfolding in the absence of denaturant, respectively. Standard deviations were obtained from the best fit of the data. To minimize the error in the fit, the rates of the fastest phase derived from the four-component fit at very low denaturant concentrations were not taken into account when comparing *raf* RBD chevron curves generated under different conditions (Figure 9A) or with different mutants (Figure 10B).

Intrinsic folding rates at 0.5 M Gdn-HCl (k_{F} 0.5 M), and intrinsic unfolding rates at 3.5 M Gdn-HCl (k_{U} 3.5 M), were obtained from a Chevron curve fit of the data points shifted to the left, such that k_{F} 0.5 M and k_{U} 3.5 M intersect the

ordinate axis. This procedure was used in order to avoid propagated errors due to extrapolation of the data in absence of denaturant. $m\text{Ubi}^{\text{F45W}}$ values at 8 °C were taken from the chevron curve reported in ref 25, while $m\text{Ubi}^{\text{F45W}}$ values measured in 0.4 M Na_2SO_4 and of the different mutants at position 26 were taken from ref 26. The two-state $k_{\text{F}}^{\text{H}_2\text{O}}$ values were not reported in the latter article because of the presence of a burst phase and rollover at low denaturant concentrations. However, on the basis of the recent demonstration that a two-state deviation in the folding of $m\text{Ubi}^{\text{F45W}}$ can be attributed to the disappearance of the fast two-state transition in the dead time of the stopped-flow experiment (28), we extrapolated $k_{\text{F}}^{\text{H}_2\text{O}}$ from the kinetic m_{F} , m_{U} , and $k_{\text{U}}^{\text{H}_2\text{O}}$ values and from the equilibrium $C_{50\%}$ values (all determined in absence of the burst phase) using eq 4:

$$k_{\text{F}}^{\text{H}_2\text{O}} = \exp[(RT \ln k_{\text{U}}^{\text{H}_2\text{O}} + m_{\text{U}}C_{50\%} + m_{\text{F}}C_{50\%})/RT] \quad (4)$$

ϕ values were calculated from both the folding ($\phi_{\text{F}} = \Delta\Delta G_{\ddagger-\text{U}}/\Delta\Delta G_{\text{F}\rightarrow\text{U}}$) and unfolding experiments ($\phi_{\text{U}} = 1 - \Delta\Delta G_{\ddagger-\text{F}}/\Delta\Delta G_{\text{F}\rightarrow\text{U}}$) by evaluating differences in the folding or unfolding free energy barrier obtained following mutation of WT amino acids to alanine. $\Delta\Delta G_{\text{F}\rightarrow\text{U}}$ was determined from unfolding equilibrium experiments.

RESULTS

Reversibility of the Folding–Unfolding Transition of yUbi and raf RBD. We first tested for the reversibility of folding and unfolding of both the Phe 45 \rightarrow Trp mutant of yUbi ($y\text{Ubi}^{\text{F45W}}$) and *raf* RBD as previously demonstrated for the human ubiquitin ($m\text{Ubi}^{\text{F45W}}$) (25). To do so, we compared the intrinsic fluorescence spectra and the unfolding free energies of the native and renatured states. Figure 2A shows that native (empty symbols) and renatured-state (filled symbols) fluorescence emission spectra are the same at a similar concentration with λ_{max} values at around 340 and 330 nm for $y\text{Ubi}^{\text{F45W}}$ (squares) and *raf* RBD (circles), respectively. On the other hand, the denatured states (6.0 M Gdn-HCl) of both proteins (dotted symbols) display very similar fluorescence spectra (with λ_{max} right shifted toward 350 nm) that are nearly identical to the fluorescence spectrum of free tryptophan in 6.0 M Gdn-HCl (\times) at an equivalent concentration. The large change in fluorescence intensity observed following denaturation of both proteins indicated that intrinsic fluorescence would provide a sensitive probe for the folding–unfolding transitions for both $y\text{Ubi}^{\text{F45W}}$ and *raf* RBD. We generated equilibrium stability curves of native (filled symbols) and renatured (empty symbols) states of both proteins by monitoring changes in the fluorescence intensity versus Gdn-HCl concentration (Figure 2B). Similar, highly cooperative fluorescence intensity transitions were obtained with midpoint concentrations of denaturation ($C_{50\%}$) of 2.88 ± 0.01 and 2.93 ± 0.02 M for $y\text{Ubi}^{\text{F45W}}$ and 2.01 ± 0.03 and 2.03 ± 0.03 M for *raf* RBD for native and renatured states, respectively. A two-state equilibrium modeling of the curves using nonlinear regression analysis of data fit to eq 1 (see Materials and Methods) revealed unfolding free energies in water ($\Delta G^{\text{H}_2\text{O}}$) of 6.4 ± 0.3 kcal/mol (native) and 6.8 ± 0.3 kcal/mol (renatured) for $y\text{Ubi}^{\text{F45W}}$ and 5.4 ± 0.7 kcal/mol (native) and 5.0 ± 0.6 kcal/mol (renatured) for *raf* RBD. These results show that native and renatured forms of both proteins display similar characteristics and further suggest

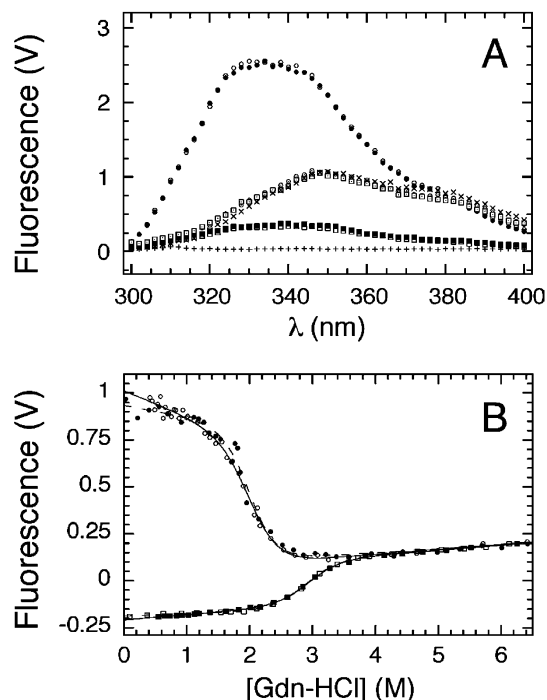


FIGURE 2: (A) Fluorescence emission spectra of yUbi^{F45W} (squares) and raf RBD (circles) in native (empty symbols, in 0.46 M Gdn-HCl), renatured (filled symbols, in 0.46 M Gdn-HCl), and denatured states (dotted symbols, in 6.0 M Gdn-HCl). Fluorescence emission spectra of free tryptophan (×) and a 6.0 M Gdn-HCl solution (+) are also shown. All sample concentrations were adjusted to 10 μM. (B) Equilibrium stability curves of native (empty symbols) and renatured (filled symbols) states of yUbi^{F45W} (squares) and raf RBD (circles) at 25 °C. Fluorescence intensities were taken from the equilibrium end points of unfolding (native) and folding (renatured) kinetic traces (10 s) using 320 and 305 nm cutoff filters for yUbi^{F45W} and raf RBD, respectively. The solid lines are results of least-squares-fit analysis of the experimental data based on a two-state folding-unfolding model; see eq 1 in Materials and Methods. The cooperativity values (*m*) and the $\Delta G^{\text{H}_2\text{O}}$ are reported in Table 1. Raw fluorescence data were transformed to set raf RBD and yUbi^{F45W} denatured-state fluorescence to the same value.

that yUbi^{F45W} and raf RBD can be unfolded and refolded in a reversible manner.

Free Energy of the Folding–Unfolding Transition of the Ubiquitin Homologues and raf RBD. The equilibrium stability curves of yUbi^{F45W} (squares) and raf RBD (circles) were then transformed into the more convenient fraction folded representation shown in Figure 3A and compared to those for mUbi^{F45W}. As shown previously by CD equilibrium experiments (38), the $C_{50\%}$ for yUbi^{F45W} was shifted to the left compared to that of mUbi^{F45W} (2.88 ± 0.01 and 3.78 ± 0.02 M Gdn-HCl, respectively; see Figure 3 and Table 1). However, despite this significant shift, the unfolding free energy of the yeast homologue extrapolated to 0 M denaturant ($\Delta G^{\text{H}_2\text{O}}$) was found to be only marginally smaller than that of mUbi^{F45W} (6.4 ± 0.3 and 7.0 ± 0.4 kcal/mol, respectively) as reflected by a larger determined *m* value for yUbi^{F45W} compared to that of mUbi^{F45W} (2.2 ± 0.1 and 1.80 ± 0.07 kcal mol⁻¹ M⁻¹, respectively; see Figure 3B). However, both ubiquitins were found to be more stable than the raf RBD (Figure 3B). The cooperativities of the transitions for both proteins, as quantified by *m* values, were similar but not identical within the experimental error for all three proteins (raf RBD having the highest value, 2.5 ± 0.3 kcal mol⁻¹ M⁻¹).

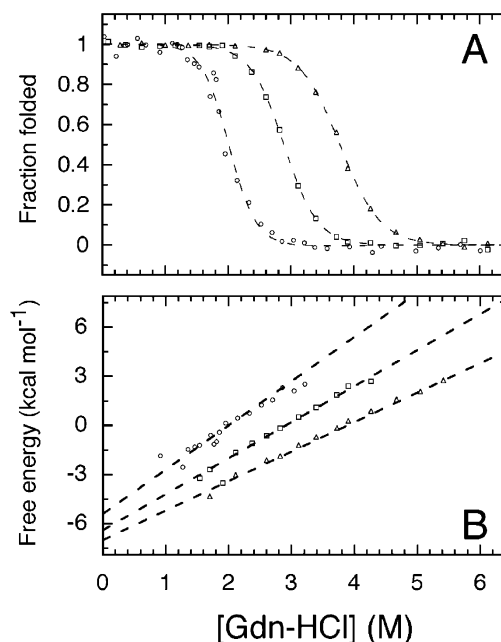


FIGURE 3: Fraction folded vs denaturant (A) and free energy of unfolding (B) of mUbi^{F45W} (Δ), yUbi^{F45W} (□), and raf RBD (○) at 25 °C. Fractional equilibrium values and free energies of unfolding were obtained by transforming equilibrium stability curves of unfolding experiments (see Figure 2B and Materials and Methods) with a two-state transition model; see eq 2. Thermodynamic parameters are reported in Table 1.

Folding and Unfolding Kinetics of the Ubiquitin Homologues and raf RBD. To characterize the kinetic behavior of mUbi^{F45W}, yUbi^{F45W}, and raf RBD, we analyzed the folding and unfolding relaxation following chemical denaturant jumps (Gdn-HCl) at 25 °C, again using the intrinsic tryptophan fluorescence as a probe. Unfolding traces could be fit to a single-exponential equation (data not shown), while up to four exponential terms were required to properly model the folding reactions. Figure 4 shows typical folding kinetic traces obtained for mUbi^{F45W}, yUbi^{F45W}, and raf RBD at various Gdn-HCl concentrations (see Materials and Methods for details). Observed intrinsic folding and unfolding rate constants (empty and filled symbols, respectively) and the amplitudes of the different folding transitions are reported in Figure 6.

To assess whether a burst phase is observed within the mixing time of the stopped-flow apparatus following initiation of folding or unfolding experiments (28), we then extrapolated the initial fluorescence values of the kinetic traces using the best-fit exponential or sum of exponential terms for each curve. Figure 5 presents both the extrapolated initial (circles) and final (squares) fluorescence intensities of all refolding and unfolding experiments performed on mUbi^{F45W}, yUbi^{F45W}, and raf RBD. For refolding experiments (empty symbols), initial fluorescence values (circles) for all three proteins showed no significant signs of deviation from the fluorescence intensity obtained for free tryptophan under similar conditions (×). For the unfolding experiments, the extrapolated initial fluorescence values (●) of all three proteins were not found to deviate from linearity. Final extrapolated fluorescence values obtained from both folding and unfolding experiments fit well to the equilibrium stability curve (solid line). Additional refolding experiments performed on raf RBD in the presence of 0.4 M Na₂SO₄ (a

Table 1: Folding Thermodynamic and Kinetic Parameters of mUbi^{F45W}, yUbi^{F45W}, and raf RBD at 25 °C Measured in Folding (f) and Unfolding (u) Experiments

			$C_{50\%}^a$	m^b	$\Delta G^{\text{H}_2\text{O}}^c$	RTm_F^d	RTm_U^d	$k_F^{\text{H}_2\text{O}}^e$	$k_U^{\text{H}_2\text{O}}^e$	β_T^f
mUbi ^{F45W}	equilibrium	f	3.76 ± 0.02	1.9 ± 0.1	7.2 ± 0.4					
		u	3.78 ± 0.02	1.80 ± 0.07	7.0 ± 0.4					
yUbi ^{F45W}	equilibrium	f	2.93 ± 0.02	2.3 ± 0.1	6.8 ± 0.3					
		u	2.88 ± 0.01	2.2 ± 0.1	6.4 ± 0.3					
raf RBD	equilibrium	f	2.03 ± 0.03	2.5 ± 0.3	5.0 ± 0.6					
		u	2.01 ± 0.03	2.7 ± 0.5	5.4 ± 0.7					
	kinetic		3.02 ± 0.04	2.15 ± 0.02	6.4 ± 0.4	1.45 ± 0.01	0.70 ± 0.01	370 ± 10	0.0078 ± 0.0008	0.67
	kinetic		1.68 ± 0.08	2.75 ± 0.06	4.9 ± 0.4	2.17 ± 0.05	0.58 ± 0.01	1100 ± 100	0.31 ± 0.03	0.79

^a The $C_{50\%}$ values are in units of moles of Gdn-HCl per liter. ^b The m values are in units of kilocalories per mole per moles of Gdn-HCl per liter. ^c The free energies of folding (ΔG) are in units of kilocalories per mole. ^d The kinetic m values for folding and unfolding (m_F and m_U , respectively) were multiplied by the factor RT (gas constant times the temperature) for the comparison with the equilibrium m values. ^e The rate constants are in units of inverse seconds. ^f The β_T values were determined from the RTm_F/m_{kin} ratio.

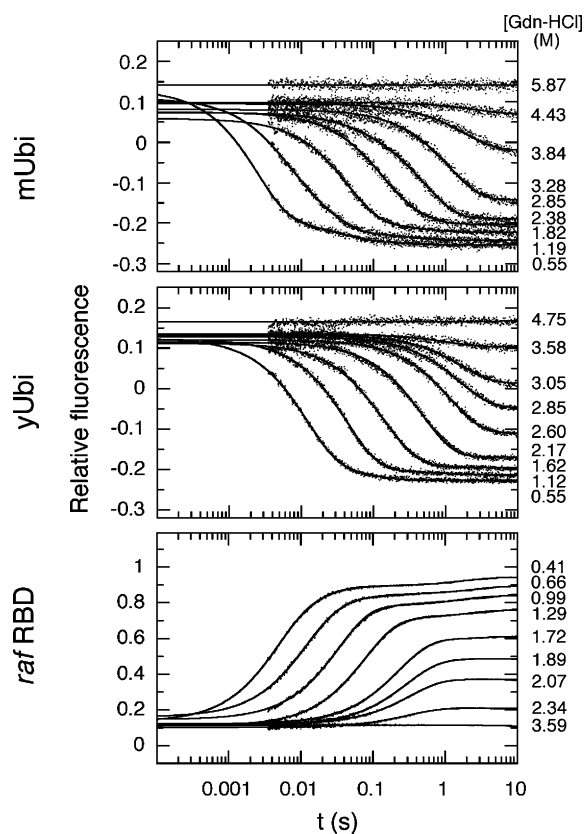


FIGURE 4: Stopped-flow kinetic refolding traces of mUbi^{F45W}, yUbi^{F45W}, and raf RBD at different denaturant concentrations. Denatured protein samples were mixed with various Gdn-HCl solutions using a 1:10 ratio. Fluorescence emission was monitored by using 320 nm (ubiquitin proteins) and 305 nm (raf RBD) cutoff filters. Kinetic traces were fit to single-exponential or multiexponential functions by using nonlinear regression analysis. The noise is reduced at the end of the raf RBD folding experiment by acquiring data in the oversampling mode (fewer acquisitions can be averaged for each point when using the logarithmic distribution of the points on the time axis).

condition known to further stabilize hydrophobic interactions) did not reveal further deviation of the initial fluorescence intensity signal on traces measured at Gdn-HCl concentrations as low as 1.5 M [relaxation folding experiments performed at a lower Gdn-HCl concentration with 0.4 M Na₂SO₄ were too fast to be analyzed with our conventional stopped-flow apparatus (28)]. These results demonstrate that for all three proteins, the intrinsic fluorescence amplitude

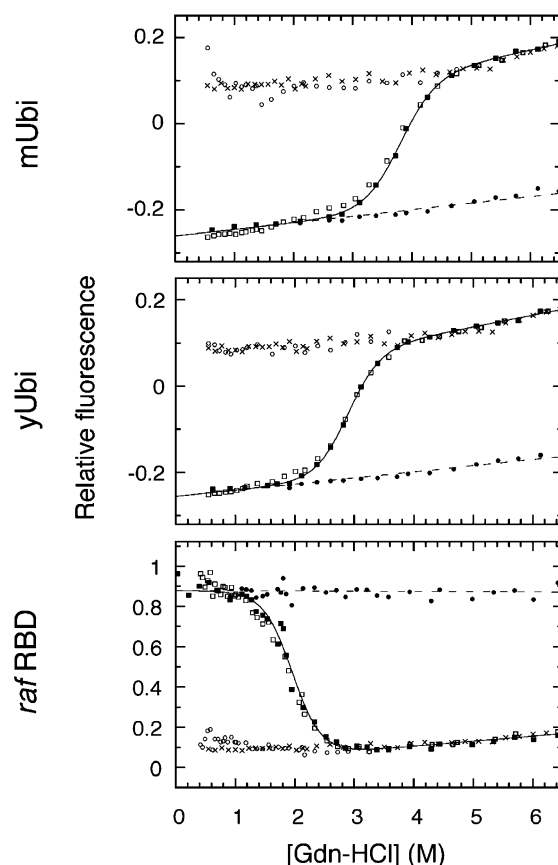


FIGURE 5: Extrapolated initial (circles) and final (squares) fluorescence intensity observed during folding (empty symbols) and unfolding (filled symbols) kinetic experiments with mUbi^{F45W}, yUbi^{F45W}, and raf RBD at 25 °C. Times signs show the fluorescence intensity of free tryptophan vs Gdn-HCl concentration. Extrapolated data were obtained from the simplest exponential functions that fit to the folding and unfolding traces (see Figure 4 and Materials and Methods). Extrapolated infinite points of unfolding experiments (filled squares) were fit to an equilibrium stability curve (eq 1). Fluorescence data obtained from the folding experiments and the free tryptophan samples were set relative to the data from unfolding experiments.

going from denatured to native states, and vice versa, can be ascribed to a series of exponential components, suggesting that there is not a rapid, sub-millisecond burst-phase intermediate for the ubiquitins or for raf RBD.

Analysis of the refolding kinetics of both mUbi^{F45W} and yUbi^{F45W}, at low Gdn-HCl concentrations (<2.4 M for

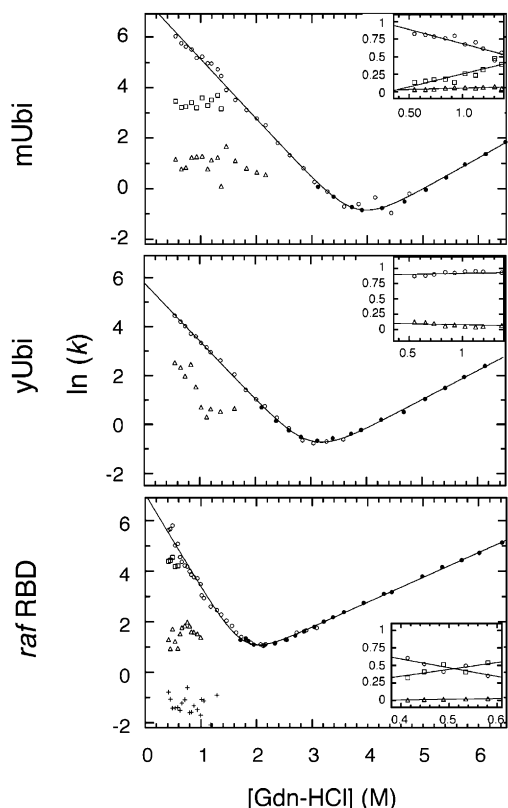


FIGURE 6: Kinetic relaxation rates of folding (empty symbols) and unfolding (filled circle) transitions of $mUbi^{F45W}$, $yUbi^{F45W}$, and raf RBD as obtained from the best fit functions of the 10 s stopped-flow kinetic traces (see Figure 4). Relative amplitudes of the folding transitions are also shown (inset) with the exception of the slowest phase for raf RBD, which displays $\sim 8\%$ of the total refolding amplitude. Circles, squares, triangles, and times signs correspond to the different observed transitions. The main transition rates of both folding and unfolding experiments were fit to a chevron equation (eq 3).

$mUbi^{F45W}$ and <1.6 M for $yUbi^{F45W}$), shows that more than one exponential term is required to properly fit the traces (Figure 6). For $mUbi^{F45W}$, approximately 80% of the total refolding amplitude occurs in a fast two-state-like transition (\circ); two slower minor phases account for the remaining amplitude (\square and \triangle ; see Figure 6). As increasing amounts of Gdn-HCl reduce the rate of the predominant fast transition, both denaturant-independent minor phases are incorporated into the same unique transition. On the other hand, the folding of $yUbi^{F45W}$ at low denaturant concentrations can be fit using the sum of only two exponentials (Figure 6): the middle transition observed in $mUbi^{F45W}$ folding (squares) is probably already incorporated in the main folding transition of $yUbi^{F45W}$, the latter being 5 times slower in the yeast homologue (1800 vs 370 s^{-1} , respectively; see $k_F^{H_2O}$ in Table 1). For both ubiquitins, observed folding rates of the main transition (\circ) match the observed unfolding rates (\bullet) around the $C_{50\%}$ values determined from the equilibrium experiments. Subsequent fitting of these observed rates to a two-state chevron curve equation (see eq 3 in Materials and Methods) showed no apparent deviation from linearity (rollover) at low or high denaturant concentrations. Finally, the thermodynamic parameters obtained from the kinetic data (Table 1) correspond well to those obtained from equilibrium measurements (although the m value obtained from the equilibrium experiment on $mUbi^{F45W}$ was found to be smaller than that

obtained from kinetic data; see the Discussion), thus suggesting that the ubiquitin homologues fold and unfold via a unique transition-state ensemble (minor folding transitions not considered; see the Discussion).

raf RBD refolding at low denaturant concentrations (<0.6 M Gdn-HCl) displays a four-phase profile (Figure 6). At 0.41 M Gdn-HCl, the fastest phase accounts for around 60% of the refolding amplitude (\circ). It is followed by three additional transitions accounting for $\sim 30\%$ (\square), $\sim 3\%$ (\triangle), and 7% (\times) of the total amplitude. As observed for $mUbi$, the folding rates of the additional transitions do not depend on denaturant concentration. The relaxation rate of the major folding transition (\circ) matches the unfolding relaxation rate (\bullet) around $C_{50\%}$ with no apparent deviation of folding and unfolding rates from the two-state chevron curve. Thermodynamic parameters obtained for raf RBD kinetic experiments (Table 1) are consistent with those obtained from the equilibrium measurements, thus suggesting that the folding and unfolding transition proceeds via a unique transition-state ensemble (minor folding transitions not considered; see the Discussion).

We then performed double-jump experiments to assess whether the additional transitions observed in $mUbi$ and raf RBD refolding could be due to a slow proline or non-prolyl amino acid isomerization event (32, 39). Re-examination of $mUbi$ refolding relaxation, acquired in oversampling mode (noise reduction strategy; compare $mUbi$ refolding traces obtained in Figure 7 versus Figure 4), revealed a fourth slow minor phase with a very low amplitude (Figure 7, $T_4 \sim 2\%$). This four-phase refolding profile obtained for both proteins is well supported by the comparison of residuals obtained from fitting the traces to three or four exponential components (see the bottom of Figure 7). From the relative amplitude of the four-component fit, it is evident that the two fastest transitions observed for both $mUbi$ and raf RBD refolding are not affected by the delay used to equilibrate the unfolded state (see the inset). However, the relative amplitude of the third transition for both proteins, and of the fourth transition for raf RBD, are significantly diminished when only 10 s is allowed for equilibration of the unfolded state after the denaturation of the native protein. Notably, all three additional transitions display similar rate constants for both proteins (see the inset, left).

Comparison of the chevron curves of all three proteins (Figure 8) reveals that the lower stability of raf RBD can be attributed to an increase of the unfolding rate [see extrapolated unfolding rates ($- -$)] rather than a decrease in the folding rate. The folding rate of raf RBD (circles) was found to be even closer to that of $mUbi^{F45W}$ (triangles) than that of $yUbi^{F45W}$ (squares). On the other hand, the denaturant dependencies of the folding and unfolding rates for the ubiquitin homologues (m_F and m_U values, respectively) displayed similar values (see Table 1). One common interpretation of kinetic m values is that they measure the relative degree of compaction of the transition-state ensemble. From the following ratio, $m_F/(m_F + m_U)$ [called the β_T value (7)], one can evaluate whether the transition state is more denatured-like or native-like. The β_T values of the ubiquitins were nearly identical (0.66 and 0.67 for $mUbi^{F45W}$ and $yUbi^{F45W}$, respectively; see Table 1) but slightly more denatured-like than that of raf RBD (0.79). However, comparable variations in β_T are observed among members

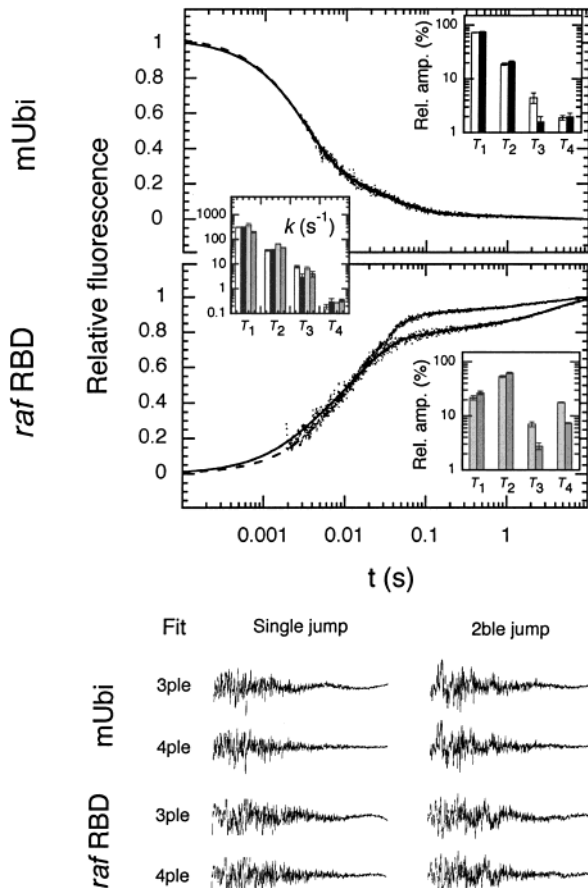


FIGURE 7: Effect of double jump (2ble-jump, rapid unfolding and refolding) on the refolding heterogeneity of His-mUbi^{F45W} (at 0.55 M Gdn-HCl) and His-*raf* RBD (at 0.82 M Gdn-HCl) at 30 °C. Acquisition of the relaxation traces in the oversampling mode revealed an additional fourth transition (T4) in the refolding of mUbi that was not detected in experiments represented in Figure 4 (see residuals of the best three- and four-exponential component fits at the bottom, 3ple and 4ple, respectively). Dashed lines (double-jump experiments) and solid lines (classic single-jump experiments) represent four exponential functions obtained from the best fits of the refolding traces. Rates (k) and amplitudes of the four transitions derived from single-jump experiments (white and light gray rectangles for mUbi and *raf* RBD, respectively) and double-jump experiments (black and dark gray, respectively) are shown as insets. Gdn-HCl concentrations and the temperature were set to obtain the best kinetic resolution of the different transitions.

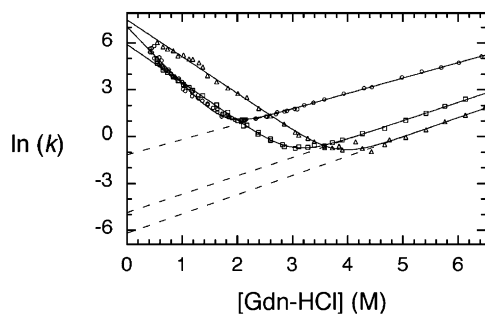


FIGURE 8: Comparative chevron curve plots of mUbi^{F45W} (Δ), yUbi^{F45W} (\square), and *raf* RBD (\circ) at 25 °C. For mUbi^{F45W}, $k_{F,H_2O} = 1800 \text{ s}^{-1}$ and $k_{U,H_2O} = 0.0021 \text{ s}^{-1}$. For yUbi^{F45W}, $k_{F,H_2O} = 370 \text{ s}^{-1}$ and $k_{U,H_2O} = 0.0078 \text{ s}^{-1}$. For *raf* RBD, $k_{F,H_2O} = 1100 \text{ s}^{-1}$ and $k_{U,H_2O} = 0.31 \text{ s}^{-1}$. See Table 1 for the complete list of the parameters obtained from the fits.

of protein families. For example, yeast, bovine, and rat ACBP have β_T values of 0.57, 0.61, and 0.69, respectively, despite

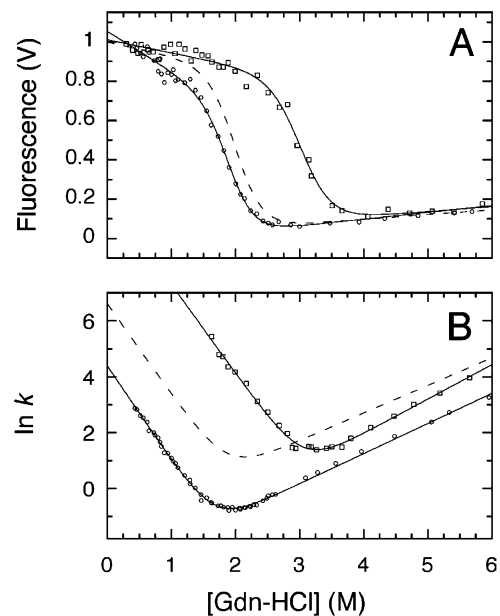


FIGURE 9: Equilibrium stability curves (A) and chevron curves (B) of *raf* RBD at 8 °C (\circ) and with 0.4 M Na₂SO₄ (\square). Fluorescence intensities are taken from the equilibrium end point of a 10 s stopped-flow refolding reaction. Dashed lines represent *raf* RBD data at 25 °C.

the fact that they are homologues (sequence more than 50% identical) (22); cold shock proteins from *Bacillus caldolyticus*, *Bacillus subtilis*, and *Thermotoga maritima* have β_T values of 0.91, 0.93, and 0.86, respectively, despite their sequences being $\sim 60\%$ identical (11).

Folding and Unfolding Kinetic Variation of raf RBD following Various Perturbations. Having established that the general folding behavior of the ubiquitins and *raf* RBD is similar, we set out to probe the folding mechanism of *raf* RBD by performing perturbation studies that had previously been performed on mUbi^{F45W}. The folding–unfolding behavior of mUbi^{F45W} has been studied with respect to temperature changes, addition of a stabilizing agent, and mutations of a central core residue (Val 26) (25, 26). We performed precisely the same studies on *raf* RBD. For the mutations, we chose the structurally equivalent position Leu 82 in *raf* RBD that corresponds to Val 26 in mUbi^{F45W} (Figure 1). Figure 9 presents *raf* RBD equilibrium stability curves (panel A) and chevron curves (panel B) at 8 °C (circles) and with 0.4 M Na₂SO₄ (squares). Under both conditions, the observed folding and unfolding rate constants of *raf* RBD fit a chevron curve and the equilibrium parameters are well estimated by the kinetic data within experimental error (see Table 2). While addition of Na₂SO₄ increases both folding rates and stabilities of the folded forms (reduction of the unfolding rate), lowering the temperature led to a reduction of the folding rate, despite also increasing the unfolding free energy barrier. Figure 10 presents the equilibrium stability curves (panel A) and chevron curves (panel B) of *raf* RBD mutants L82A (\circ), L82V (\square), and L82I (\bullet). All mutants display apparent two-state unfolding transitions with m values similar to that of the WT protein (see Table 2). From the equilibrium stability curves (Figure 10A), we observed that all mutants appear to be less stable than WT *raf* RBD (see Table 2). The reduction in stability for mutants L82I (\bullet) and L82V (\square) was caused by an

Table 2: Folding Thermodynamic and Kinetic Parameters of *raf* RBD at 8 °C with 0.4 M Na₂SO₄ and of *raf* RBD with Different Central Core Residues at Position 82

		m^a	$\Delta G^{H_2O}{}^b$	RTm_F^a	RTm_U^a	$k_F^{0.5M}{}^c$	$k_U^{3.5M}{}^c$	$\Delta\Delta G_{\ddagger\rightarrow U}^d$	$\Delta\Delta G_{\ddagger\rightarrow F}^e$
25 °C	equilibrium	2.7 ± 0.5	5.4 ± 0.7						
	kinetic	2.51 ± 0.06	4.66 ± 0.08	1.92 ± 0.04	0.59 ± 0.01	148 ± 7	9.2 ± 0.2	—	—
8 °C	equilibrium	2.7 ± 0.3	5.3 ± 0.6						
	kinetic	2.50 ± 0.02	4.1 ± 0.1	2.01 ± 0.02	0.64 ± 0.01	14.9 ± 0.4	2.05 ± 0.03	1.45 ± 0.04	0.91 ± 0.02
Na ₂ SO ₄	equilibrium	3.3 ± 0.7	10 ± 2						
	kinetic	2.57 ± 0.08	7.5 ± 0.1	1.83 ± 0.05	0.73 ± 0.03	7000 ± 1000	3.9 ± 0.2	-2.3 ± 0.1	0.51 ± 0.04
L82I	equilibrium	2.3 ± 0.2	3.7 ± 0.4						
	kinetic	2.7 ± 0.1	3.6 ± 0.2	2.06 ± 0.09	0.63 ± 0.02	240 ± 20	90 ± 3	-0.29 ± 0.08	-1.35 ± 0.03
L82V	equilibrium	2.6 ± 0.4	3.6 ± 0.6						
	kinetic	2.52 ± 0.08	2.7 ± 0.2	1.83 ± 0.07	0.69 ± 0.01	88 ± 3	160 ± 5	0.31 ± 0.05	-1.69 ± 0.03
L82A	equilibrium	2.55 ± 0.08	1.15 ± 0.03						
	kinetic	2.6 ± 0.2	0.4 ± 0.2	1.7 ± 0.1	0.89 ± 0.02	5.2 ± 0.4	440 ± 30	1.98 ± 0.07	-2.29 ± 0.05

^a The m values are in units of kilocalories per mole per moles of Gdn-HCl per liter. ^b The free energies of folding (ΔG) are in units of kilocalories per mole. Kinetic ΔG values were determined by adding $\Delta\Delta G_{\ddagger\rightarrow F}$ and subtracting $\Delta\Delta G_{\ddagger\rightarrow U}$ from the WT kinetic ΔG . ^c The intrinsic rate constants are in units of inverse seconds. To avoid error propagation resulting from extrapolation, the rate of folding (k_F) is reported at 0.5 M Gdn-HCl and the rate of unfolding (k_U) is reported at 3.5 M Gdn-HCl. ^d $\Delta\Delta G_{\ddagger\rightarrow U}$ with a mutation or change in conditions (x) = $(RT \ln k_F^{0.5M})_{wt(25^\circ C)} - (RT \ln k_F^{0.5M})_x$. ^e $\Delta\Delta G_{\ddagger\rightarrow F}$ with a mutation or change in conditions (x) = $(RT \ln k_U^{3.5M})_{wt(25^\circ C)} - (RT \ln k_U^{3.5M})_x$.

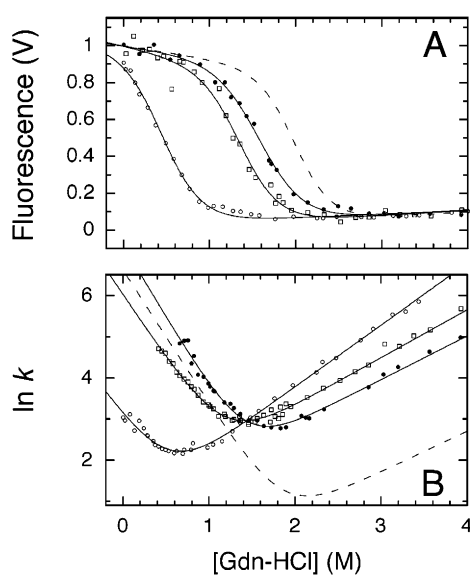


FIGURE 10: Equilibrium stability curves (A) and chevron curves (B) of *raf* RBD mutants L82I (●), L82V (□), and L82A (○). All samples were adjusted for an after-mixing concentration of 15 μ M (except for the L82A mutant which was at $\sim 5 \mu$ M for unfolding experiments). Fluorescence intensities are the equilibrium end points of a 10 s stopped-flow unfolding reaction. The dashed line represents the WT *raf* RBD equilibrium and chevron curves at 25 °C.

increase in the unfolding rates, while the lower stability of L82A could be attributed to both a decrease and an increase of its folding and unfolding rates, respectively.

Figure 11 summarizes the effect of the different mutations performed at an equivalent central core residue on both *raf* RBD (gray) and mUbi^{F45W} (white) (see Materials and Methods for details on the extrapolation of the two-state folding transition rate of mUbi^{F45W} mutants). Free energy differences in the height of the folding (Figure 11A) and unfolding (Figure 11B) barriers obtained at 8 °C and with 0.4 M Na₂SO₄ are also shown. The key result revealed here is that folding free energy barriers for both *raf* RBD and mUbi^{F45W} are perturbed in the same manner (Figure 11A): (1) at lower temperatures ($\Delta\Delta G_{\ddagger\rightarrow U}$ values obtained from the difference between $\Delta G_{\ddagger\rightarrow U}$ at 8 °C and that at 25 °C are 1.45 ± 0.04 and 1.45 kcal/mol, respectively), (2) by the

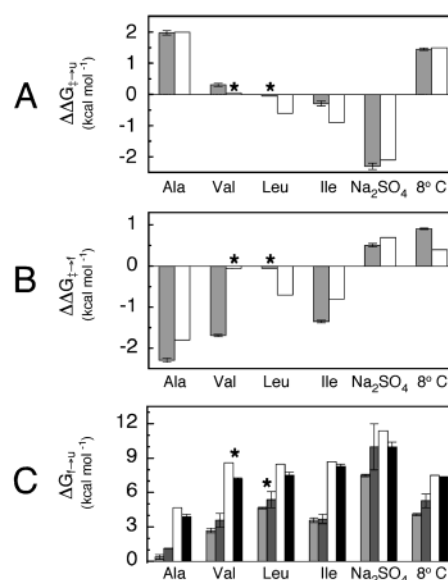


FIGURE 11: Comparison of differences in the free energy barrier of folding (A) and unfolding (B) obtained when various perturbations are used to affect folding-unfolding pathways for both *raf* RBD (gray rectangles) and mUbi (white rectangles; data taken from refs 25 and 26). Mutations to Ala, Val, Leu, and Ile are introduced on a structurally equivalent position in both proteins (see Figure 1). The Na₂SO₄ concentration was 0.4 M. (C) Free energies of unfolding extrapolated from the kinetic $\Delta\Delta G$ values (light gray and white for *raf* RBD and mUbi, respectively) or measured from the equilibrium curves (dark gray and black for *raf* RBD and mUbi, respectively) are compared.

stabilizing agent ($\Delta\Delta G_{\ddagger\rightarrow U}$ values obtained from the difference between $\Delta G_{\ddagger\rightarrow U}$ in the presence and absence of 0.4 M Na₂SO₄ are -2.3 ± 0.1 and -2.1 kcal/mol, respectively), and (3) by mutations at a structurally equivalent position. For both proteins, the fastest folding mutant was the isoleucine substitution, followed by leucine, valine, and alanine, for the last of which folding was found to be even slower than in the WT proteins at 8 °C ($\Delta\Delta G_{\ddagger\rightarrow U}$ for the mutation to alanine = 1.98 ± 0.07 and 2.0 kcal/mol for *raf* RBD and mUbi^{F45W}, respectively). Interestingly, faster folding mutants of both proteins are not the most stable; unfolding experiments reveal that the unfolding free energy barrier is maximal for the naturally selected amino acid

(indicated by asterisks in Figure 11B). Northey and co-workers reported similar results in a study on an SH3 domain. They demonstrated that the folding rate could be significantly accelerated by replacing amino acids located at positions that are loosely packed in the transition state ($\phi < 0.3$) with those having bulkier side chains even though these mutations reduce the stability of the native state (40).

DISCUSSION

Ubiquitin Homologues and raf RBD Fold and Unfold via an Apparent Two-State Mechanism. We have demonstrated that the folding and unfolding of ubiquitin homologues mUbi and yUbi and ubiquitin superfamily member raf RBD can be described well by an apparent two-state mechanism. This conclusion is supported by four observations: (1) the convergence of observed folding and unfolding rate constants around the equilibrium-determined $C_{50\%}$ (Figure 6, shoulder region), (2) the absence of rollover in the chevron curve at both low and high denaturant concentrations (Figures 6 and 7), (3) the absence of any relevant burst phase observed in the folding and unfolding process (Figure 5), and (4) the similar extrapolation of the thermodynamic parameters for the folding–unfolding transition from the kinetic and equilibrium experiments (Table 1). Thus, mUbi results obtained from our study are in good agreement with the recent study of Krantz and Sosnick (28) in which careful analysis of the fast refolding trace of mUbi^{F45W} acquired within the detection limit of the stopped-flow apparatus shows no burst phase under conditions where an intermediate has been suggested to exist (25, 26). However, it is interesting to note that the equilibrium experiment performed with mUbi^{F45W} yielded smaller-than-expected m values (1.80 ± 0.07 and 1.9 ± 0.1 kcal mol⁻¹ M⁻¹ for the unfolding and refolding end point experiments, respectively, compared to 2.13 ± 0.04 kcal mol⁻¹ M⁻¹ for the kinetic experiment). This slight discrepancy was not observed for yUbi^{F45W} for which both folding (2.3 ± 0.1 kcal mol⁻¹ M⁻¹) and unfolding (2.2 ± 0.1 kcal mol⁻¹ M⁻¹) equilibrium-determined m values were similar to those extrapolated from kinetic data (2.15 ± 0.02 kcal mol⁻¹ M⁻¹). By using various probes, Khorasanizadeh and co-workers also obtained equilibrium-determined m values smaller than those determined from kinetic experiments (2.2 kcal mol⁻¹ M⁻¹) (25): 1.9 ± 0.1 kcal mol⁻¹ M⁻¹ using fluorescence at 353 nm, 1.9 ± 0.1 kcal mol⁻¹ M⁻¹ using NMR peaks of His 68 CH₂, and 2.0 ± 0.1 kcal mol⁻¹ M⁻¹ using molar ellipticity at 222 nm. On the other hand, Krantz and Sosnick found similar m values under the same conditions in both their equilibrium and kinetic experiments: 2.18 ± 0.02 kcal mol⁻¹ M⁻¹ (CD equilibrium experiments) and 2.17 ± 0.04 kcal mol⁻¹ M⁻¹, respectively (28).

Similar Folding Heterogeneity in the Refolding of the Ubiquitins, and raf RBD. As demonstrated earlier, the folding mechanism of raf RBD and yUbi^{F45W} can be described well as a two-state process when considering only the major fastest refolding transition. However, many additional minor phases are also observed during the refolding of both proteins at low denaturant concentrations. In their folding studies with mUbi^{F45W}, Khorasanizadeh and co-workers also observed two slower and smaller-amplitude transitions during the first 100 s of the folding relaxation traces (26). For both transitions, rate constants decreased with an increase in the denaturant

concentration (from 40 to 10 s⁻¹ and from 0.4 to 0.025 s⁻¹ for the middle and slowest transitions, respectively). In contrast to these results, Krantz and Sosnick reported from their two-state analysis that three to five exponential terms were needed to properly fit the data over an extended time range (28). In both reports, minor phases were proposed to be due to small populations of slowly refolding molecules with *cis*-prolyl peptide bonds preceding proline residues [mUbi contains three prolines in its coding sequence (Pro 19, Pro 37, and Pro 38)]. In the study presented here, four exponential terms were required to model the refolding kinetic traces of mUbi^{F45W} and raf RBD at low denaturant concentrations during the first 10 s (Figure 7). The additional transitions observed in both proteins were found to have similar rate constants and were relatively insensitive to Gdn-HCl [Figure 7 (inset, left) and Figure 6]. Furthermore, double-jump experiments suggest that the second transition observed during the refolding of both proteins does not display the characteristics of a prolyl *cis*–*trans* isomerization. Its amplitude is similar even when the protein is refolded from a nearly homogeneous population of all-*trans* amino acid conformations. However, the third transition in both proteins displays the characteristics of a slowly refolding population containing *cis* peptide bonds preceding non-prolyl residues. Its rate (~ 8 and ~ 7 s⁻¹ for mUbi and raf RBD, respectively), amplitude (4.5 and 7.1%, respectively), and dependence on equilibration time are similar to the behavior of a transition first described by Pappenberger and colleagues (39). The fourth transition observed for raf RBD also appeared to be sensitive to equilibrium time, and displayed a rate and an amplitude that are characteristic of prolyl *cis*–*trans* isomerization (32). No such amplitude variation could be observed for the slowest transition of mUbi. However, it is relevant to note that this later phase remained hardly detectable because of both its low rate constant and relatively small amplitude. Finally, it is interesting to note that a previous pulse deuterium–hydrogen exchange experiment (41) has already characterized three minor phases in the refolding of mUbi, which have rate constants similar to the three minor transitions identified in this study. In this study, amide hydrogen exchanges of residues 59, 61, and 69 were protected at a significantly slower rate (~ 45 s⁻¹) than the majority of the other amide protons, whereas amide protons of almost all amino acids also had $\sim 12\%$ of their complete amplitude protected at a rate of 7 s⁻¹. A fourth minor phase, accounting for $\sim 8\%$ of the complete protection amplitude for most protons, was also identified with a rate constant as slow as 0.07 s⁻¹. More experiments are needed to determine whether the second transition observed in both mUbi and raf RBD refolding could represent a late intermediate accumulating along the folding pathway (29).

The Ubiquitins and raf RBD: The Same Fold and a Similar Folding Rate and Mechanism. As discussed by Plaxco and colleagues, no cases have been reported for which a homologous set of proteins exhibits folding rates that differ by more than 1 order of magnitude when their stabilities are taken into account (4). However, conservation of folding rate and mechanism within proteins displaying sequence homology could also be linked to the conservation of key folding residues (42). Thus, to further explore the extent to which folding behavior of a protein is determined by the complexity of its fold rather than by the fine details of its sequence,

kinetic studies of more structural homologues with unrelated sequences must be experimentally compared.

In the study presented here, we demonstrate that both structurally related *raf* RBD and the ubiquitin homologues fold and unfold via an apparent two-state model with relatively similar folding rates. In an attempt to compare the folding mechanism of sequence-unrelated *raf* RBD to that of mUbi, we then showed that very similar folding free energy variation was observed when both proteins are folded at lower temperatures, with added stabilizing agent, or when similar amino acids are inserted at a structurally equivalent position. ϕ value analysis performed on the structurally equivalent position in both proteins yields similar medium values as determined from substituting WT amino acids with alanine (0.47 or 0.46 for *raf* RBD, 0.63 or 0.44 for mUbi^{F45W} using $\Delta\Delta G_{\ddagger-U}$ or $\Delta\Delta G_{\ddagger-F}$, respectively; see Table 2). Such values suggest that the central buried amino acid in the α -helices of both proteins displays approximately half of its native stability in the transition state. These observations suggest that, in addition to their similar folding rate constants, *raf* RBD and the ubiquitins also fold via similar mechanisms.

How Insensitive Are Folding Rates and Pathways to Fine Sequence Details? The results presented above provide a clear example of folding rate and mechanism conservation within ubiquitin superfold members. However, no apparent fine sequence detail conservation can be observed in the alignment of mUbi and *raf* RBD primary structure (Figure 1). Other comparative studies of structurally similar but not obviously homologous proteins have also led to similar conclusions. Chiti and co-workers showed that the transition states of the topologically related human muscle acylphosphatase (Acp) and activation domain of procarboxypeptidase A2 (ADA2h) have remarkably similar structures, despite their very low level of sequence identity (13%) (14). The authors also showed that large folding rate differences between these proteins (0.24 and 900 s⁻¹, respectively) were consistent with their relative contact order values. Baker and co-workers elegantly showed that structurally related proteins L and G (sequences 15% identical) possess two similar and nearly isoenergetic folding pathways (43–45). Clarke and co-workers suggested that the folding pathway of Ig-like proteins shares common features, based on a strong correlation they observed between the folding rates and stabilities of many members with levels of sequence identity of less than 12% (46). However, this study also illustrated the non-negligible contribution of fine sequence details (interactions defining the structure and stability of a fold) in determining the folding rates of the Ig-like proteins (FNfn9 and FNfn10 display 3 orders of magnitude of folding rate variation). Finally, Guerois and Serrano's research on Sso7d, a protein displaying the characteristic SH3 fold but lacking sequence identity with these other proteins, also suggests that not only the topology but also the particular sequence of a protein could sometimes be responsible for the selection of folding pathways (in the case of Sso7d, a glycine rich region located in the fifth β -strand) (47). Generalization of ϕ value analysis to the entire sequence of both *raf* RBD and mUbi and the folding characterization of additional sequence-unrelated ubiquitin-like proteins will certainly provide further evidence of the relative insensitivity of folding rates and mechanisms of proteins to fine sequence.

ACKNOWLEDGMENT

The yUbi cDNA and *raf* RBD coding sequence were kindly provided by Dr. Nils Johnsson (Max-Delbruck-Laboratorium, Koln, Germany) and Dr. Julie E Scheffler (Bristol-Myers Squibb Pharmaceutical Research Institute, Princeton, NJ), respectively. We acknowledge François-Xavier Campbell-Valois and Dr. Melissa L. Lerch for critical reading of the manuscript, members of the Michnick group for helpful discussions, and professor Jeffrey W. Keillor for providing access to the stopped-flow apparatus.

REFERENCES

- Baker, D. (2000) A surprising simplicity to protein folding, *Nature* 405, 39–42.
- Baldwin, R. L., and Rose, G. D. (1999) Is protein folding hierarchic? II. Folding intermediates and transition states, *Trends Biochem. Sci.* 24, 77–83.
- Baldwin, R. L., and Rose, G. D. (1999) Is protein folding hierarchic? I. Local structure and peptide folding, *Trends Biochem. Sci.* 24, 26–33.
- Plaxco, K. W., Simons, K. T., Ruczinski, I., and Baker, D. (2000) Topology, stability, sequence, and length: defining the determinants of two-state protein folding kinetics, *Biochemistry* 39, 11177–11183.
- Dobson, C. M., and Karplus, M. (1999) The fundamentals of protein folding: bringing together theory and experiment, *Curr. Opin. Struct. Biol.* 9, 92–101.
- Eaton, W. A., Munoz, V., Hagen, S. J., Jas, G. S., Lapidus, L. J., Henry, E. R., and Hofrichter, J. (2000) Fast kinetics and mechanisms in protein folding, *Annu. Rev. Biophys. Biomol. Struct.* 29, 327–359.
- Fersht, A. R. (1999) *Structure and mechanism in protein science: a guide to enzyme catalysis and protein folding*, Freeman, New York.
- Jackson, S. E. (1998) How do small single-domain proteins fold? *Folding Des.* 3, R81–R91.
- Myers, J. K., and Oas, T. G. (2002) Mechanism of fast protein folding, *Annu. Rev. Biochem.* 71, 783–815.
- Plaxco, K. W., Simons, K. T., and Baker, D. (1998) Contact order, transition state placement and the refolding rates of single domain proteins, *J. Mol. Biol.* 277, 985–994.
- Perl, D., Welker, C., Schindler, T., Schroder, K., Marahiel, M. A., Jaenicke, R., and Schmid, F. X. (1998) Conservation of rapid two-state folding in mesophilic, thermophilic and hyperthermophilic cold shock proteins, *Nat. Struct. Biol.* 5, 229–235.
- Kim, D. E., Gu, H., and Baker, D. (1998) The sequences of small proteins are not extensively optimized for rapid folding by natural selection, *Proc. Natl. Acad. Sci. U.S.A.* 95, 4982–4986.
- Riddle, D. S., Santiago, J. V., Bray-Hall, S. T., Doshi, N., Grantcharova, V. P., Yi, Q., and Baker, D. (1997) Functional rapidly folding proteins from simplified amino acid sequences, *Nat. Struct. Biol.* 4, 805–809.
- Chiti, F., Taddei, N., White, P. M., Bucciantini, M., Magherini, F., Stefani, M., and Dobson, C. M. (1999) Mutational analysis of acylphosphatase suggests the importance of topology and contact order in protein folding, *Nat. Struct. Biol.* 6, 1005–1009.
- Martinez, J. C., and Serrano, L. (1999) The folding transition state between SH3 domains is conformationally restricted and evolutionarily conserved, *Nat. Struct. Biol.* 6, 1010–1016.
- Riddle, D. S., Grantcharova, V. P., Santiago, J. V., Alm, E., Ruczinski, I., and Baker, D. (1999) Experiment and theory highlight role of native state topology in SH3 folding, *Nat. Struct. Biol.* 6, 1016–1024.
- Alm, E., and Baker, D. (1999) Prediction of protein-folding mechanisms from free-energy landscapes derived from native structures, *Proc. Natl. Acad. Sci. U.S.A.* 96, 11305–11310.
- Galzitskaya, O. V., and Finkelstein, A. V. (1999) A theoretical search for folding/unfolding nuclei in three-dimensional protein structures, *Proc. Natl. Acad. Sci. U.S.A.* 96, 11299–11304.
- Munoz, V., and Eaton, W. A. (1999) A simple model for calculating the kinetics of protein folding from three-dimensional structures, *Proc. Natl. Acad. Sci. U.S.A.* 96, 11311–11316.
- Larson, S. M., Ruczinski, I., Davidson, A. R., Baker, D., and Plaxco, K. W. (2002) Residues participating in the protein folding

- nucleus do not exhibit preferential evolutionary conservation, *J. Mol. Biol.* 316, 225–233.
21. Ferguson, N., Capaldi, A. P., James, R., Kleanthous, C., and Radford, S. E. (1999) Rapid folding with and without populated intermediates in the homologous four-helix proteins Im7 and Im9, *J. Mol. Biol.* 286, 1597–1608.
 22. Kragelund, B. B., Hojrup, P., Jensen, M. S., Schjerling, C. K., Juul, E., Knudsen, J., and Poulsen, F. M. (1996) Fast and one-step folding of closely and distantly related homologous proteins of a four-helix bundle family, *J. Mol. Biol.* 256, 187–200.
 23. Mayer, R. J., Landon, M., and Layfield, R. (1998) Ubiquitin superfolds: intrinsic and attachable regulators of cellular activities? *Folding Des.* 3, R97–R99.
 24. Murzin, A. G., Brenner, S. E., Hubbard, T., and Chothia, C. (1995) SCOP: a structural classification of proteins database for the investigation of sequences and structures, *J. Mol. Biol.* 247, 536–540.
 25. Khorasanizadeh, S., Peters, I. D., Butt, T. R., and Roder, H. (1993) Folding and stability of a tryptophan-containing mutant of ubiquitin, *Biochemistry* 32, 7054–7063.
 26. Khorasanizadeh, S., Peters, I. D., and Roder, H. (1996) Evidence for a three-state model of protein folding from kinetic analysis of ubiquitin variants with altered core residues, *Nat. Struct. Biol.* 3, 193–205.
 27. Roder, H., and Colon, W. (1997) Kinetic role of early intermediates in protein folding, *Curr. Opin. Struct. Biol.* 7, 15–28.
 28. Krantz, B. A., and Sosnick, T. R. (2000) Distinguishing between two-state and three-state models for ubiquitin folding, *Biochemistry* 39, 11696–11701.
 29. Krantz, B. A., Mayne, L., Rumbley, J., Englander, S. W., and Sosnick, T. R. (2002) Fast and slow intermediate accumulation and the initial barrier mechanism in protein folding, *J. Mol. Biol.* 324, 359–371.
 30. Emerson, S. D., Madison, V. S., Palermo, R. E., Waugh, D. S., Scheffler, J. E., Tsao, K. L., Kiefer, S. E., Liu, S. P., and Fry, D. C. (1995) Solution structure of the Ras-binding domain of c-Raf-1 and identification of its Ras interaction surface, *Biochemistry* 34, 6911–6918.
 31. Holm, L., and Sander, C. (1996) Mapping the protein universe, *Science* 273, 595–603.
 32. Brandts, J. F., Halvorson, H. R., and Brennan, M. (1975) Consideration of the possibility that the slow step in protein denaturation reactions is due to cis–trans isomerism of proline residues, *Biochemistry* 14, 4953–4963.
 33. Johnsson, N., and Varshavsky, A. (1994) Ubiquitin-assisted dissection of protein transport across membranes, *EMBO J.* 13, 2686–2698.
 34. Picard, V., Ersdal-Badju, E., Lu, A., and Bock, S. C. (1994) A rapid and efficient one-tube PCR-based mutagenesis technique using Pfu DNA polymerase, *Nucleic Acids Res.* 22, 2587–2591.
 35. Scheffler, J. E., Waugh, D. S., Bekesi, E., Kiefer, S. E., LoSardo, J. E., Neri, A., Prinzo, K. M., Tsao, K. L., Wegrzynski, B., Emerson, S. D., et al. (1994) Characterization of a 78-residue fragment of c-Raf-1 that comprises a minimal binding domain for the interaction with Ras-GTP, *J. Biol. Chem.* 269, 22340–22346.
 36. Pace, C. N., Vajdos, F., Fee, L., Grimsley, G., and Gray, T. (1995) How to measure and predict the molar absorption coefficient of a protein, *Protein Sci.* 4, 2411–2423.
 37. Peterman, B. F. (1979) Measurement of the dead time of a fluorescence stopped-flow instrument, *Anal. Biochem.* 93, 442–444.
 38. Ibarra-Molero, B., Loladze, V. V., Makhatazde, G. I., and Sanchez-Ruiz, J. M. (1999) Thermal versus guanidine-induced unfolding of ubiquitin. An analysis in terms of the contributions from charge–charge interactions to protein stability, *Biochemistry* 38, 8138–8149.
 39. Pappenberger, G., Aygun, H., Engels, J. W., Reimer, U., Fischer, G., and Kiefhaber, T. (2001) Nonprolyl cis peptide bonds in unfolded proteins cause complex folding kinetics, *Nat. Struct. Biol.* 8, 452–458.
 40. Northey, J. G., Di Nardo, A. A., and Davidson, A. R. (2002) Hydrophobic core packing in the SH3 domain folding transition state, *Nat. Struct. Biol.* 9, 126–130.
 41. Briggs, M. S., and Roder, H. (1992) Early hydrogen-bonding events in the folding reaction of ubiquitin, *Proc. Natl. Acad. Sci. U.S.A.* 89, 2017–2021.
 42. Mirny, L., and Shakhnovich, E. (2001) Evolutionary conservation of the folding nucleus, *J. Mol. Biol.* 308, 123–129.
 43. Nauli, S., Kuhlman, B., and Baker, D. (2001) Computer-based redesign of a protein folding pathway, *Nat. Struct. Biol.* 8, 602–605.
 44. Kuhlman, B., O'Neill, J. W., Kim, D. E., Zhang, K. Y., and Baker, D. (2002) Accurate computer-based design of a new backbone conformation in the second turn of protein L, *J. Mol. Biol.* 315, 471–477.
 45. Alm, E., Morozov, A. V., Kortemme, T., and Baker, D. (2002) Simple physical models connect theory and experiment in protein folding kinetics, *J. Mol. Biol.* 322, 463–476.
 46. Clarke, J., Cota, E., Fowler, S. B., and Hamill, S. J. (1999) Folding studies of immunoglobulin-like beta-sandwich proteins suggest that they share a common folding pathway, *Struct. Folding Des.* 7, 1145–1153.
 47. Guerois, R., and Serrano, L. (2000) The SH3-fold family: experimental evidence and prediction of variations in the folding pathways, *J. Mol. Biol.* 304, 967–982.
 48. Laskowski, R. A. (2001) PDBsum: summaries and analyses of PDB structures, *Nucleic Acids Res.* 29, 221–222.

BI0359426